Electronic Supplementary Information

Densely-packed hybrid films comprising SnO_2 and reduced graphite oxide for high-density electrochemical capacitors

Segi Byun[*], *Byungha Shin*[*]

Department of Materials Science and Engineering, Korea Advanced Institute of Science and Technology, Daejeon, 34141, Republic of Korea

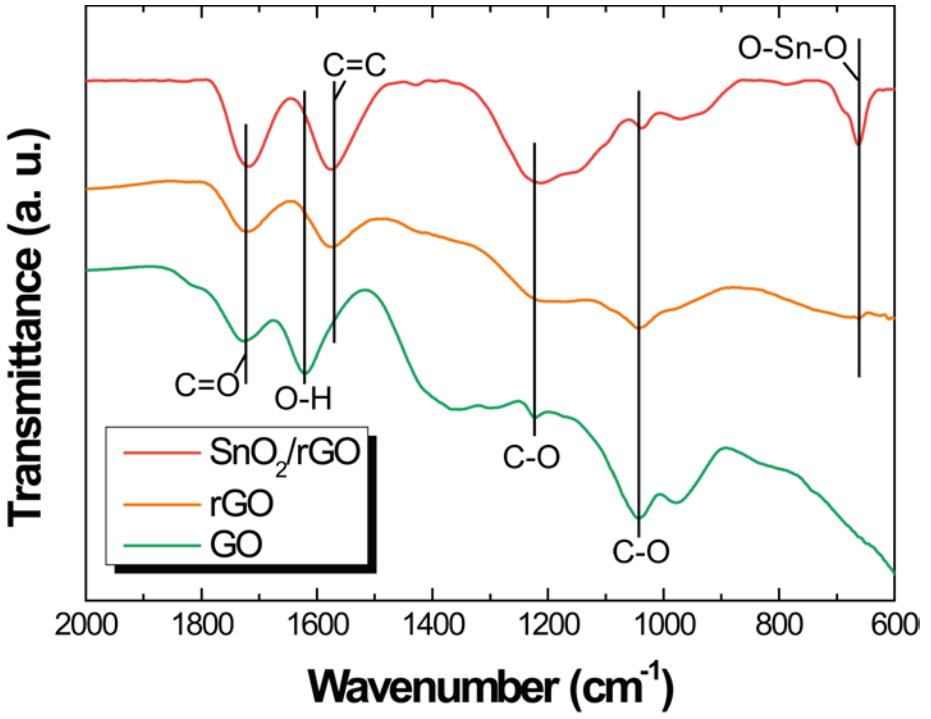

Fig. S1 FT-IR spectra of GO, rGO and SnO_2/rGO hybrid films. Even after thermal reduction at 200 °C, the hydroxyl group of GO were mostly eliminated, but carboxyl (C–O and C=O) remained inside the rGO film. The various peaks in the figure indicate that the carboxylic stretching vibration, O–H bending vibration, sp^2 carbon, epoxide C–O stretching, alkoxy C–O bonding, O–Sn–O symmetric stretching located at 1729, 1619, 1577, 1224, 1045, and 665 cm^{-1}, respectively.[1-4]

There is a study regarding the formation of SnO_2 NPs on multi-walled carbon nanotubes using a simple chemistry.[5] This work proposed a possible reaction mechanism between $SnCl_2$ and O_2

(dissolved in the water) in HCl solution. From this proposed reaction, it is deduced that oxygen species in the reaction would be originated from oxygen functional groups of GO. As examined by FT-IR spectra, SnO_2/rGO hybrid had much less hydroxyl groups than other functional groups such as carboxyl and epoxide groups. Therefore, it is deduced that one of the oxygen functional groups, especially, hydroxyl group (–OH) might be mainly bound with Sn^{2+} ions to form SnO_2 NPs on GO sheets. From our investigation, the possible reaction mechanism of the chemical redox reaction between GO and the $SnCl_2$ precursor will be proposed as follows:

$$O_2 \text{ (from GO)} + 2SnCl_2 + 2H_2O \rightarrow 2SnO_2 \text{ (on GO)} + 4HCl$$

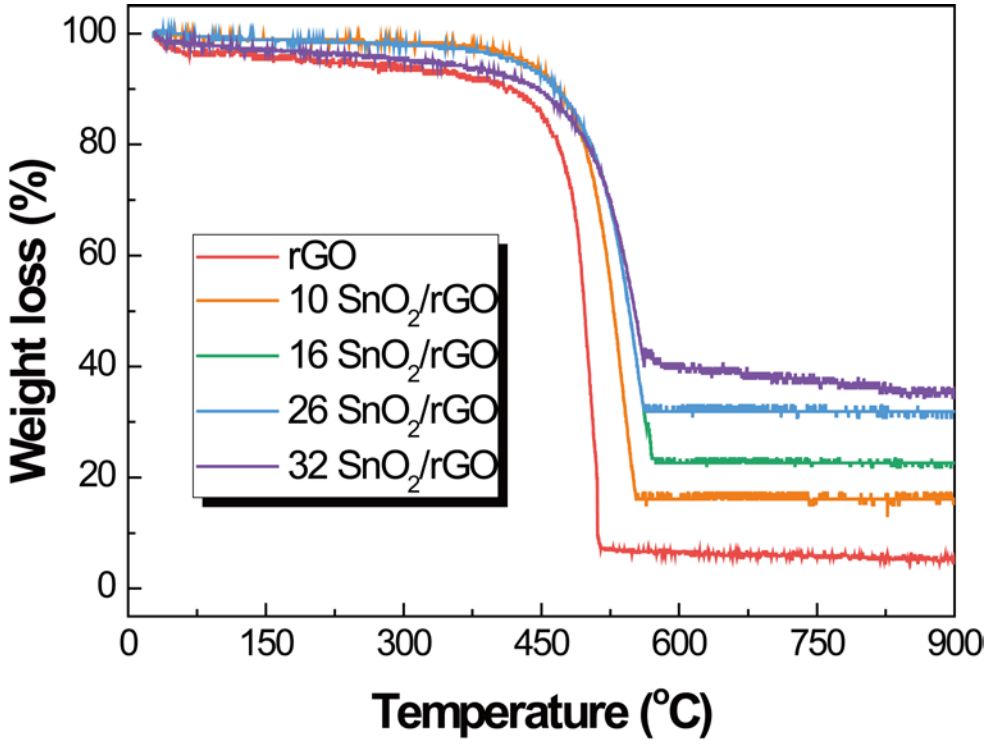

Fig. S2 Thermal gravimetric analysis for bare rGO and various SnO_2/rGO films. The x (10, 16, 26, and 32) weight percent of SnO_2 in the hybrid is described as the x SnO_2/rGO.

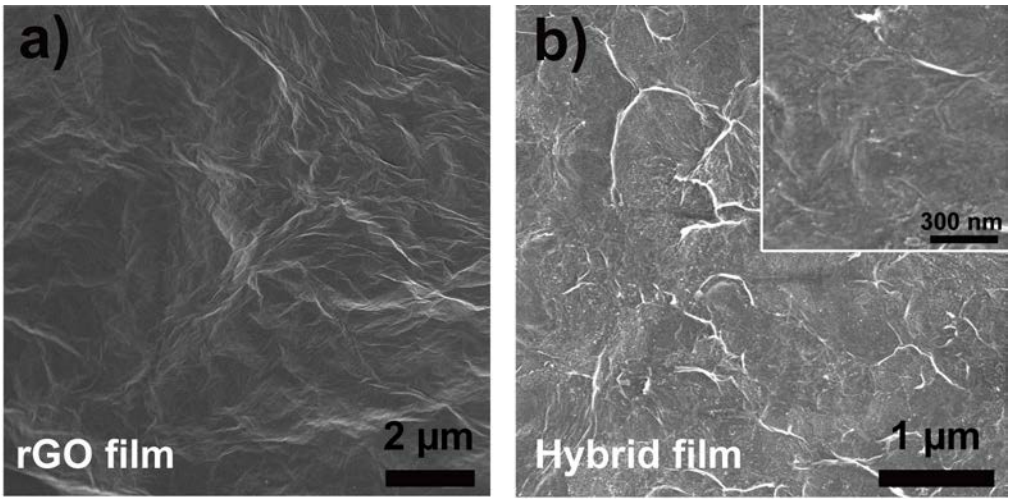

Fig. S3 SEM images of the surfaces of the (a) rGO and (b) SnO_2/rGO films. A magnified image of the hybrid film is shown in the inset of Figure S1b. The hybrid film exhibited a sheet morphology that was similar to that of the rGO film, but the hybrid film contained some wrinkles due to the presence of the SnO_2 NPs in the rGO sheets.

Table S1. Material information for bare rGO and various SnO_2/rGO films.

Sample	Mass (mg)	Area (cm^2)	Thickness (μm)	Volume (10^{-4} cm^3)	Packing Density (g/cm^3)	Electrical Conductivity (S/m)
rGO	0.34	1.33	2.34	3.11	1.09	172.0 ± 15.2
10 SnO_2/rGO	0.54	1.33	2.42	3.22	1.68	139.0 ± 31.4
16 SnO_2/rGO	0.65	1.33	2.56	3.39	1.92	54.94 ± 1.0
26 SnO_2/rGO	0.91	1.33	3.05	4.05	2.25	34.9 ± 3.1

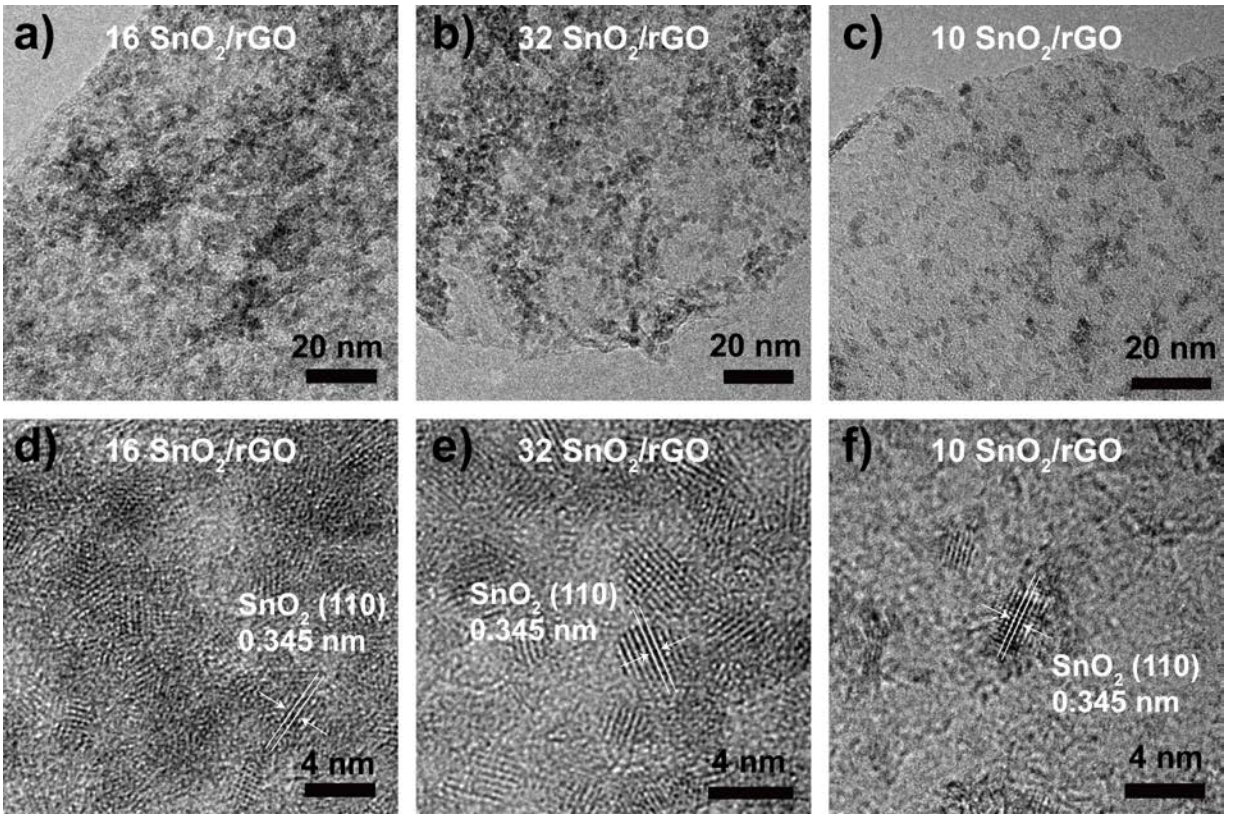

Fig. S4 TEM images of the surfaces of various SnO_2/rGO hybrids. (a) 16 SnO_2/rGO, (b) 32 SnO_2/rGO and (c) 10 SnO_2/rGO. High-resolution TEM images of each sample are shown in (d), (e), and (f), respectively. The images indicate that sub-5-nm-diameter SnO_2 particles were formed on the rGO surfaces.

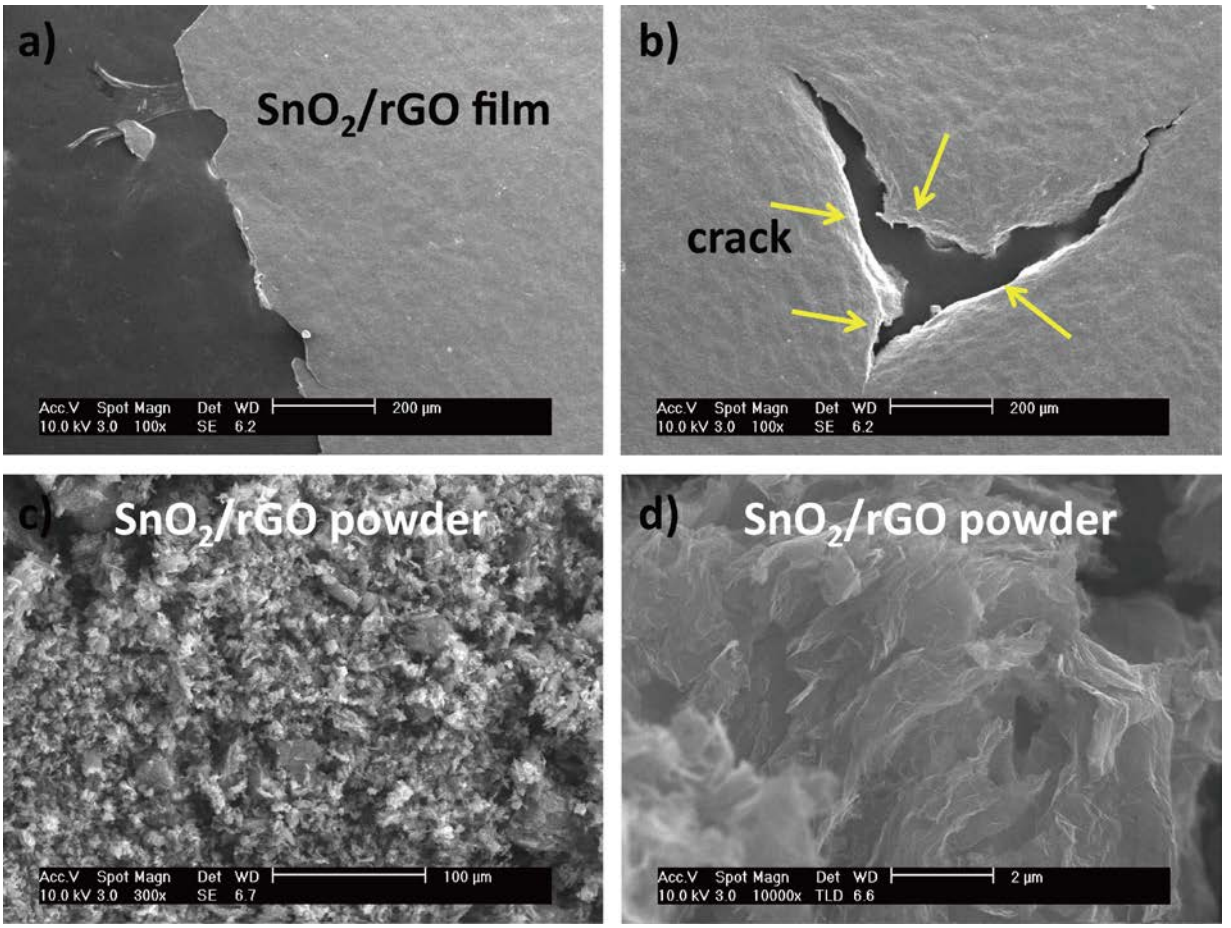

Fig. S5 SEM images of various forms of SnO_2/rGO hybrids. (a) 16 SnO_2/rGO hybrid film, (b) a region of the cracked 32 SnO_2/rGO film, (c) a powder form of SnO_2/rGO and (d) its magnified region.

The SnO_2 NPs were uniformly decorated on both the rGO surfaces and edges, and they formed a compact film structure below 32 wt% SnO_2 in the hybrid (Fig. S5a). However, as seen in the Fig. S5b, cracks were observed in the SnO_2/rGO film with 32 wt % SnO_2, and furthermore, above 32 wt % SnO_2 in the hybrid, SnO2/rGO hybrid started to be aggregated into particles as seen in the Fig. S5c–d. Although the powder form of SnO_2/rGO had a different morphology than other hybrids below 32 wt% SnO_2, it showed still uniform distribution of SnO_2 NPs in the hybrids, supported by the elemental mapping images of the Fig. S6.

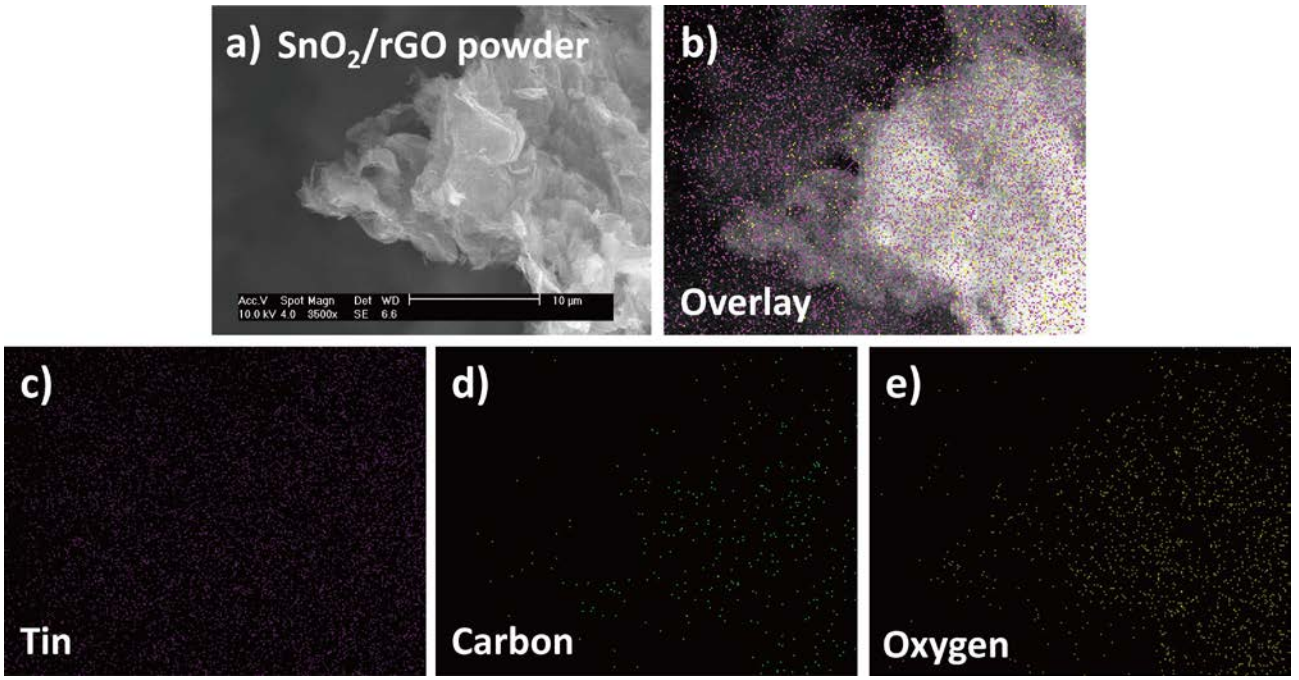

Fig. S6 (a) SEM image of the powder form of SnO_2/rGO hybrid. Energy-dispersive X-ray spectroscopy (EDS) elemental mapping of the hybrid; (b) overlay, (c) tin (pink dots), (d) carbon (green dots), and (e) oxygen (yellow dots) elemental mapping images.

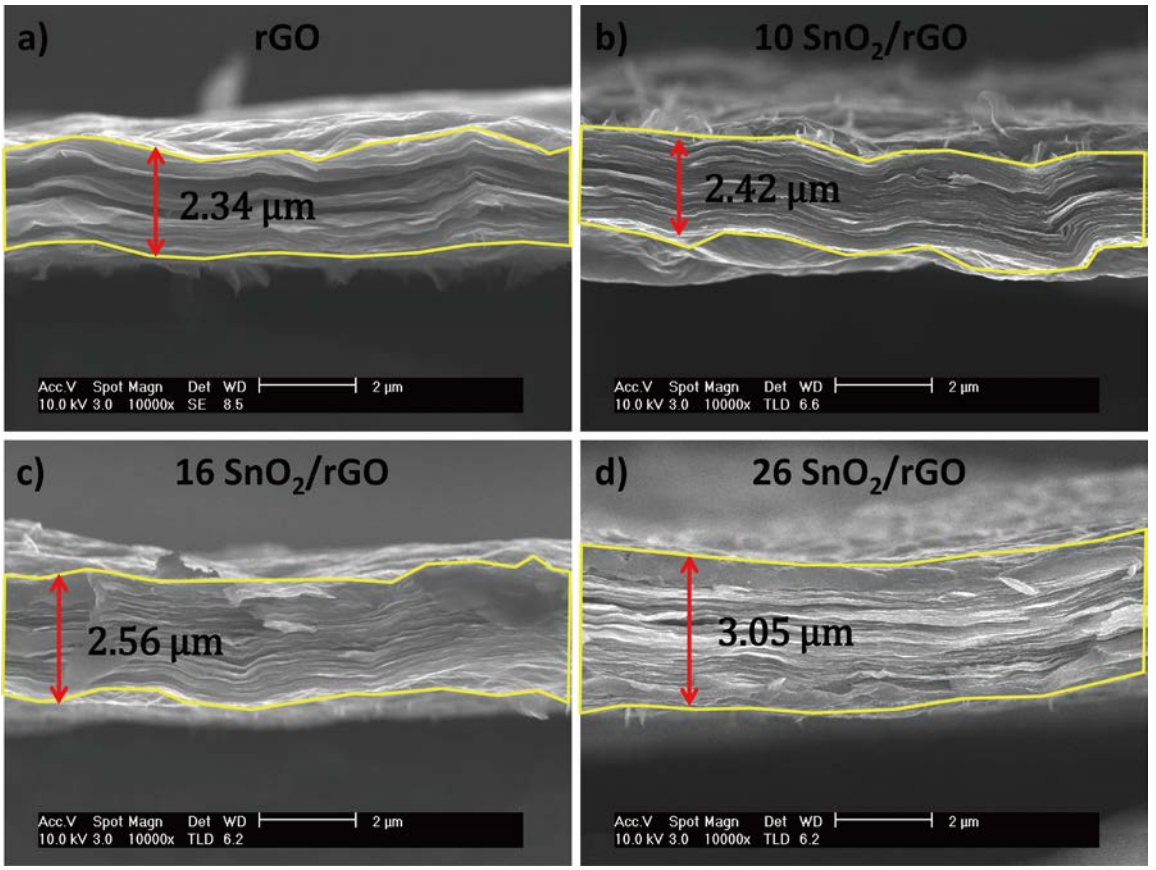

Fig. S7 Cross-sectional SEM images of the rGO and various SnO_2/rGO compact films. The film thicknesses of each film were estimated from the areas bounded by the yellow lines divided by the film length (ca. 11.7 µm).

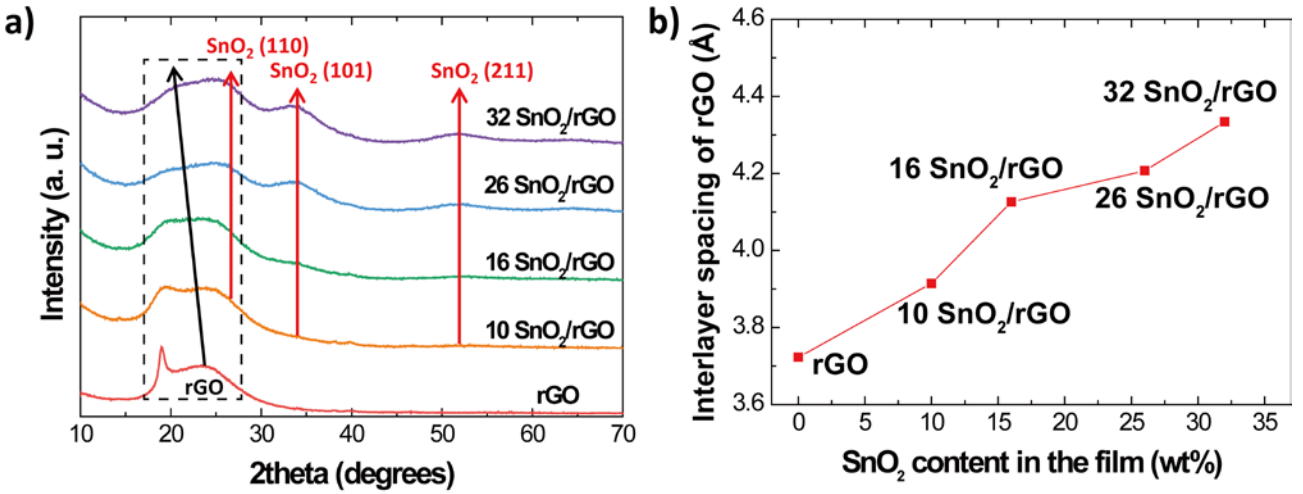

Fig. S8 (a) XRD spectra of the rGO and SnO_2/rGO compact films. For the 32 SnO_2/rGO, a large piece of the cracked film was selected for the XRD measurement. The SnO_2 peaks indicated by red arrows correspond to cassiterite SnO_2 peaks; these were in good agreement with JCPDS No. 41–1445. The black line indicates the rGO peaks, and (b) the estimated rGO interlayer spacing was increased as introducing more SnO_2 NPs in the hybrids. This indicates the role of SnO_2 NPs acting as effective spacers to prevent the restacking of rGO sheets.

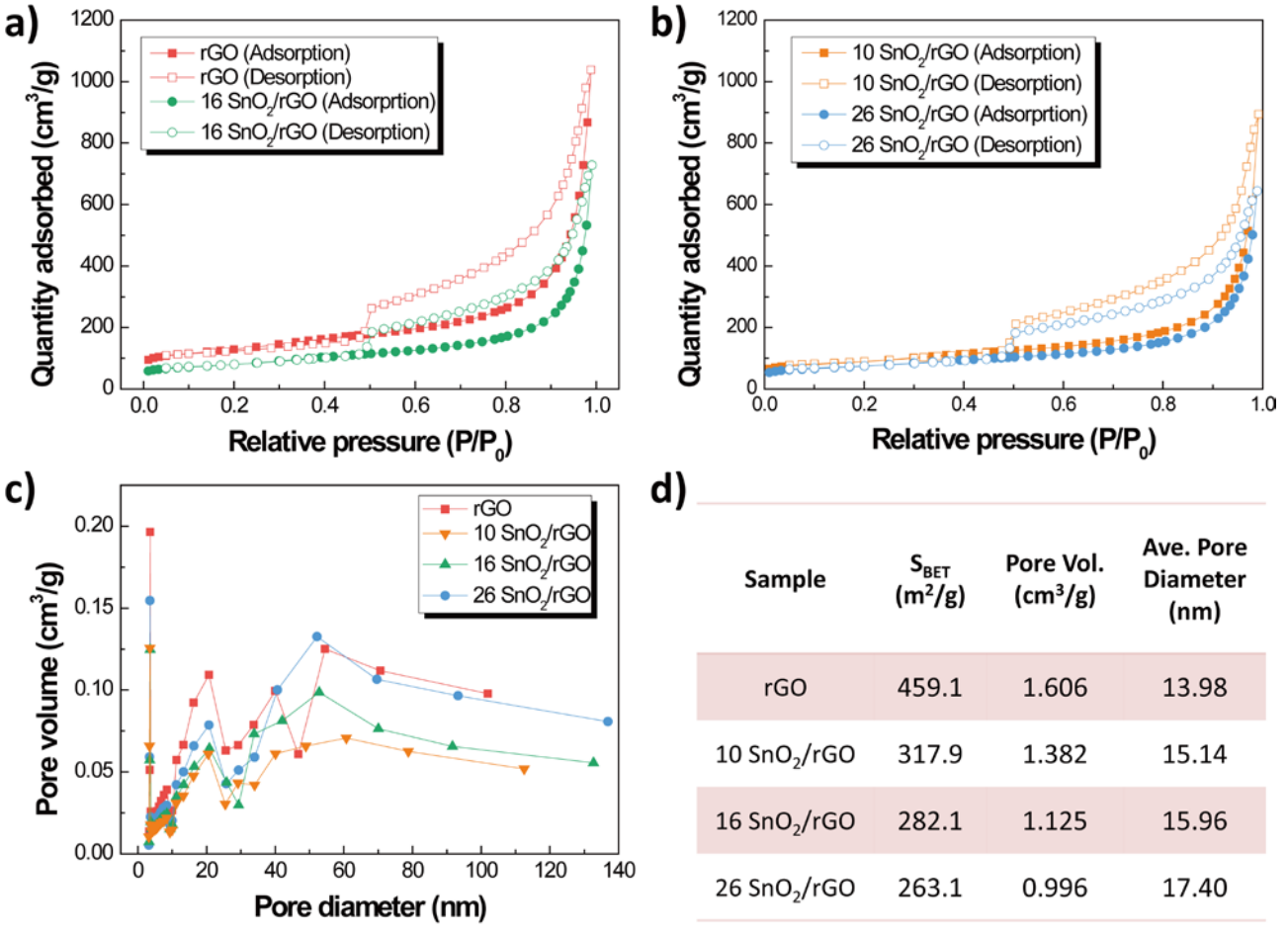

Sample	S_{BET} (m^2/g)	Pore Vol. (cm^3/g)	Ave. Pore Diameter (nm)
rGO	459.1	1.606	13.98
10 SnO_2/rGO	317.9	1.382	15.14
16 SnO_2/rGO	282.1	1.125	15.96
26 SnO_2/rGO	263.1	0.996	17.40

Fig. S9 (a–b) BET N_2 adsorption-desorption isotherms of the rGO and various SnO_2/rGO films. (c) The corresponding BJH pore size distribution curves of all samples, and (d) summarized surface area characterization results.

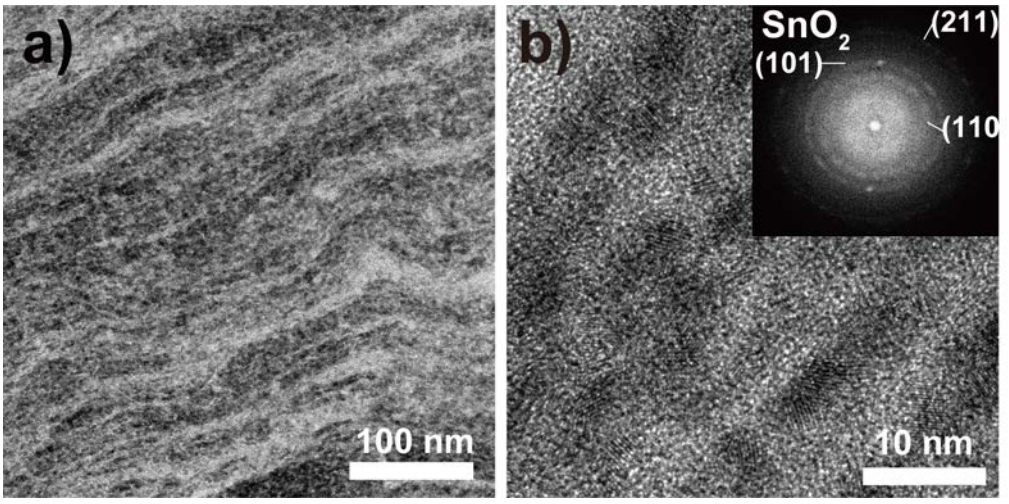

Fig. S10 Cross-sectional TEM images of the 16 SnO_2/rGO film. (a) Low- and (b) high-resolution images. The inset of (b) is a typical selected area electron diffraction (SAED) pattern of polycrystalline SnO_2 nanoparticles.

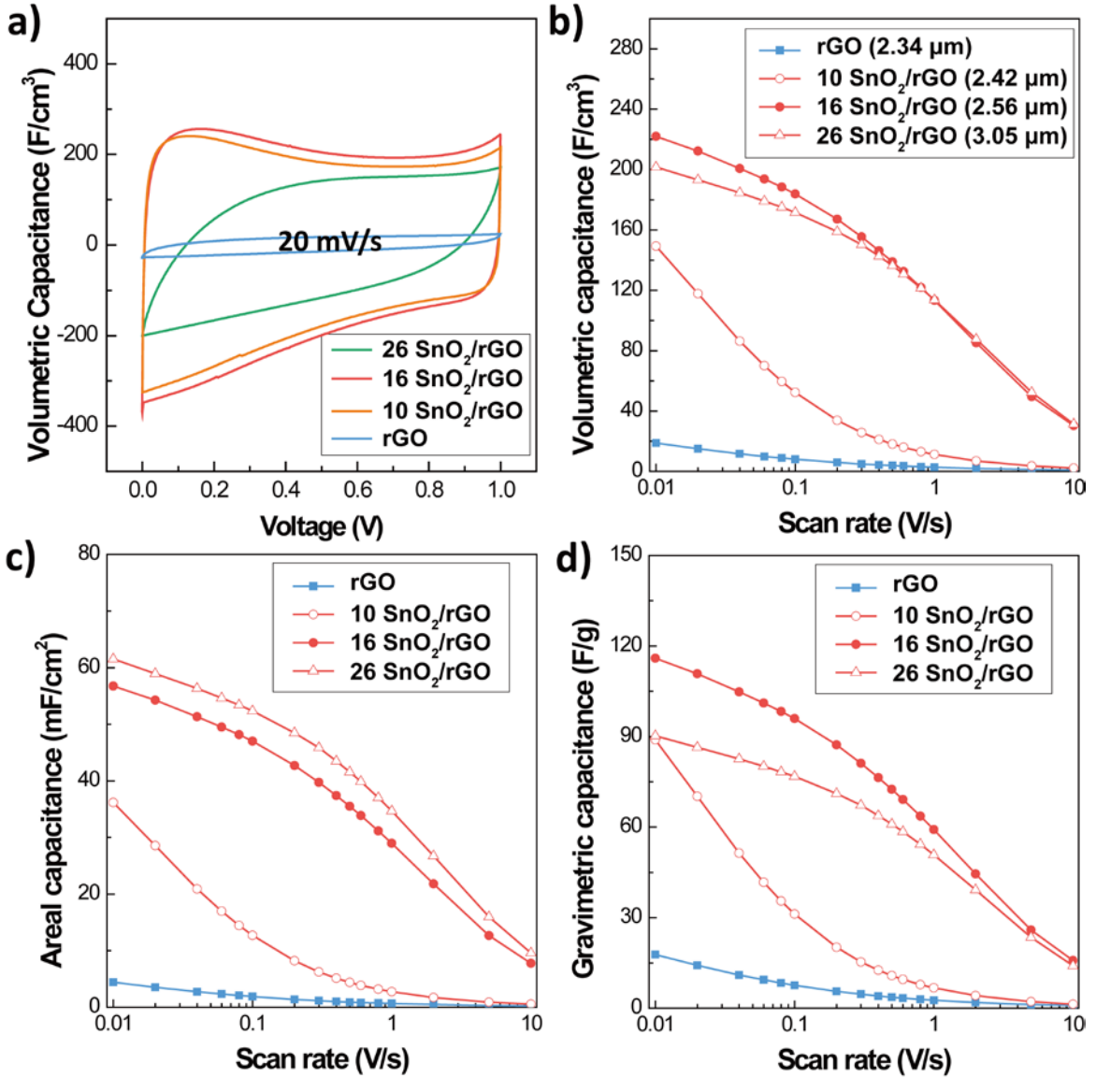

Fig. S11 (a) CV curves of the various SnO_2/rGO hybrid films at 20 mV s^{-1}. (b) Volumetric, (c) areal and (d) gravimetric capacitances of the various SnO_2/rGO films as a function of scan rate. These tests were conducted in an acidic electrolyte of 1 M H_2SO_4.

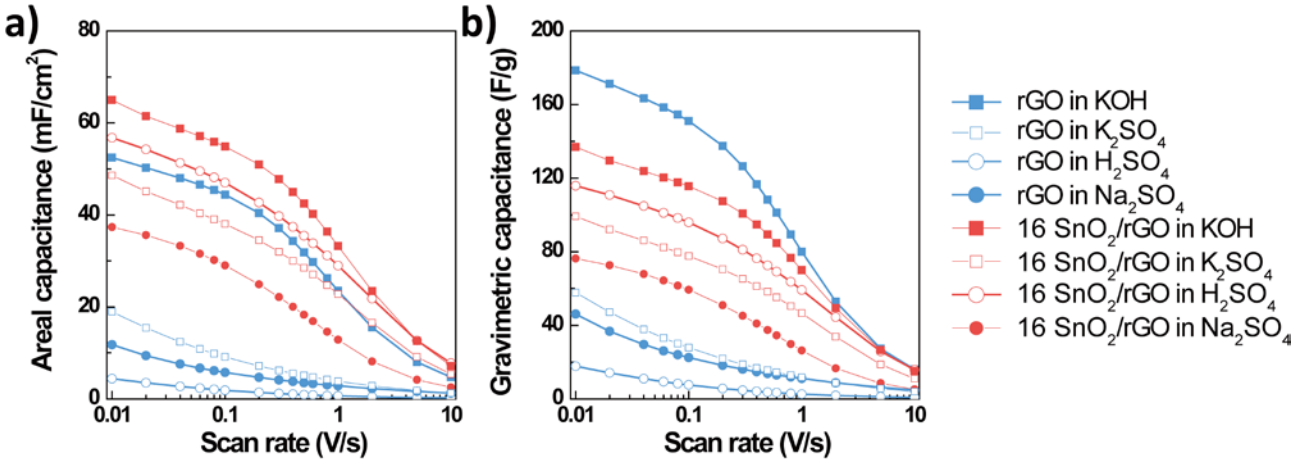

Fig. S12 (a) Areal and (b) gravimetric capacitances of bare rGO and 16 SnO_2/rGO in different electrolytes.

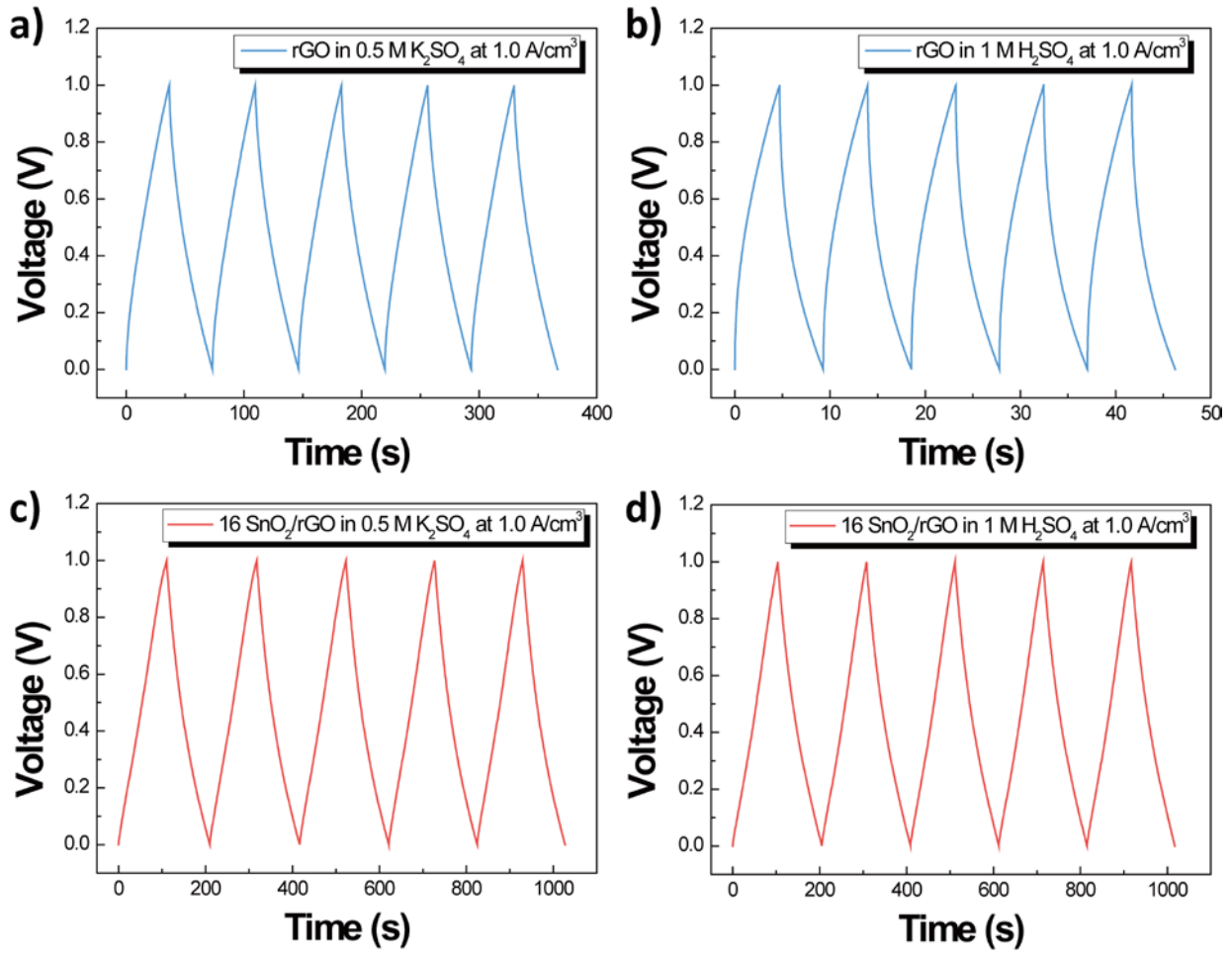

Fig. S13 Charge/discharge curves of the (a–b) rGO and (c-d) optimized SnO_2/rGO films in acidic and neutral electrolytes.

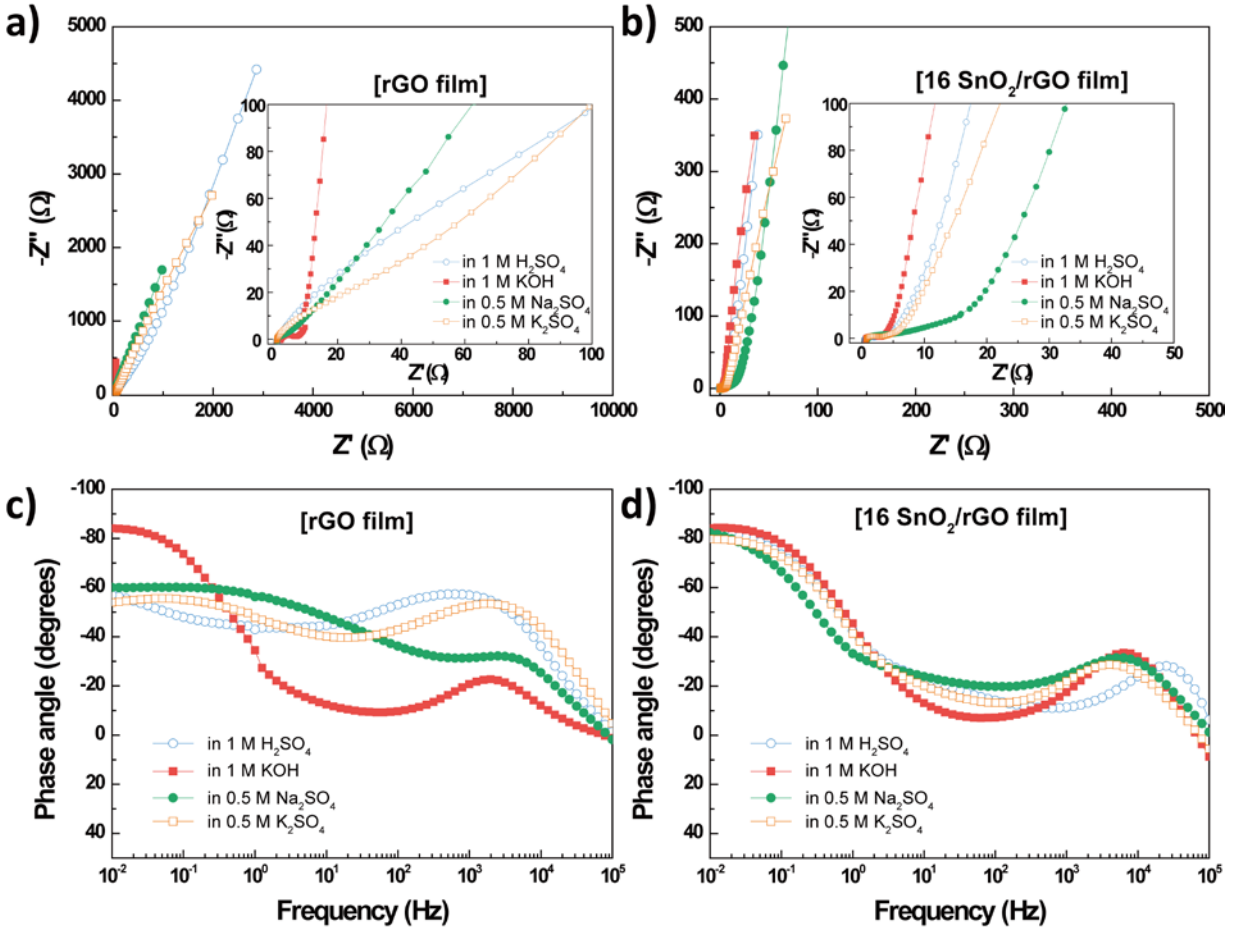

Fig. S14 Nyquist plots of (a) rGO and (b) optimized SnO_2/rGO films in various aqueous electrolytes. The insets correspond to the high frequency regions. The corresponding Bode plots of the (c) rGO and (d) optimized SnO_2/rGO films. The 16 SnO_2/rGO film exhibited a greatly enhanced ion transport property in various aqueous electrolytes compared with the bare rGO film.

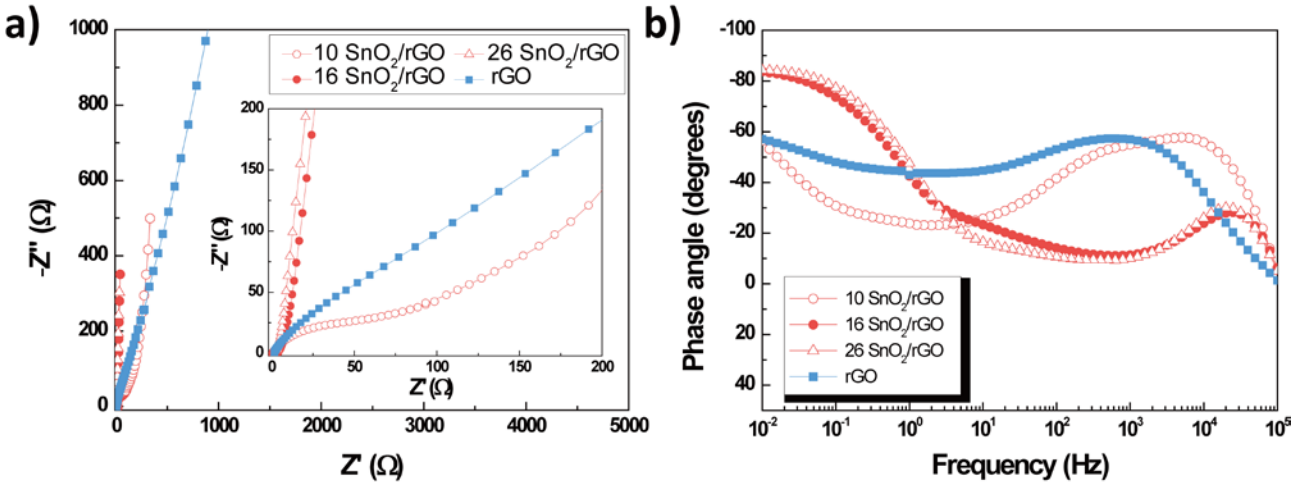

Fig. S15 (a) Nyquist and (b) Bode plots of various SnO_2/rGO films in an acidic electrolyte of 1 M H_2SO_4. The inset corresponds to the high frequency region of the Nyquist plot. These plots indicated that the optimum loading amount of SnO_2 in the hybrid was ca. 16–26 wt% SnO_2.

Table S2. Detailed Nyquist plot fitting results for rGO and 16 SnO_2/rGO films.

Sample	R_s (Ω)	R_{ct} (Ω)	R_{ESR} (Ω)	C_{dl} (mF)
rGO in H_2SO_4	1.50	61.01	62.51	0.27
rGO in K_2SO_4	0.91	16.16	17.07	6.98
rGO in Na_2SO_4	0.99	85.20	86.19	1.93
rGO in KOH	0.65	1.56	2.21	83.20
16 SnO_2/rGO in H_2SO_4	0.69	2.34	3.03	52.39
16 SnO_2/rGO in K_2SO_4	0.89	2.33	3.22	49.53
16 SnO_2/rGO in Na_2SO_4	0.95	5.86	6.81	38.28
16 SnO_2/rGO in KOH	0.74	1.98	2.72	79.06

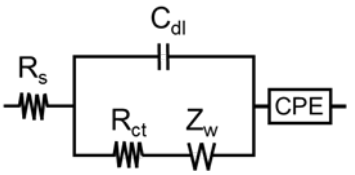

Fig. S16 Equivalent circuit for fitting of the Nyquist plot for the bare rGO and SnO_2/rGO films. R_s: solution resistance, R_{ct}: charge transfer resistance, C_{dl}: double layer capacitance, CPE: constant phase element, Z_w: Warburg impedance.

Supplementary References

1 A. Kumar, L. Rout, R. S. Dhaka, S. L. Samal and P. Dash, *RSC Advances*, 2015, **5**, 39193.

2 J. I. Paredes, S. Villar-Rodil, A. Martínez-Alonso and J. M. D. Tascón, *Langmuir*, 2008, **24**, 10560.

3 W. Gu, W. Zhang, X. Li, H. Zhu, J. Wei, Z. Li, Q. Shu, C. Wang, K. Wang, W. Shen, F. Kang and D. Wu, *J. Mater. Chem.*, 2009, **19**, 3367.

4 X. Tong, H. Wang, G. Wang, L. Wan, Z. Ren, J. Bai and J. Bai, *J. Solid State Chem.*, 2011, **184**, 982.

5 H.-T. Fang, X. Sun, L.-H. Qian, D.-W. Wang, F. Li, Y. Chu, F.-P. Wang and H.-M. Cheng, *J. Phys. Chem. C*, 2008, **112**, 5790.